Molecular BioSystems

Interfacing chemical biology with the -omic sciences and systems biology

www.molecularbiosystems.org

Volume 9 | Number 9 | September 2013 | Pages 2171–2392

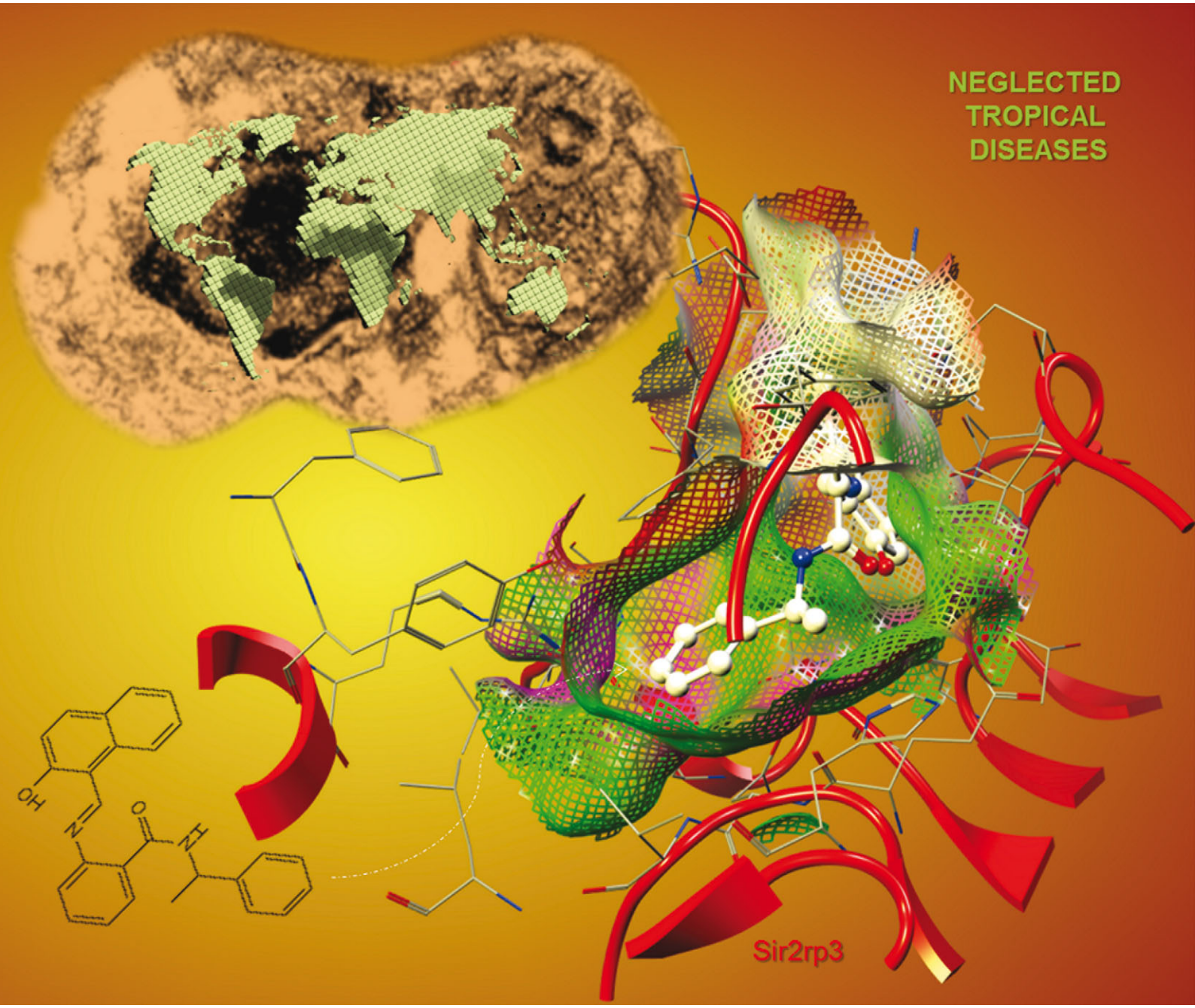

ISSN 1742-206X

RSC Publishing

PAPER

Alessandra Nurisso *et al.*

Structural insights of SIR2rp3 proteins as promising biotargets to fight against Chagas disease and leishmaniasis

Molecular BioSystems

RSC Publishing

PAPER

View Article Online
View Journal | View Issue

Cite this: *Mol. BioSyst.*, 2013, **9**, 2223

Structural insights of SIR2rp3 proteins as promising biotargets to fight against Chagas disease and leishmaniasis†

Lionel Sacconnay,[a] Despina Smirlis,[b] Emerson Ferreira Queiroz,[a] Jean L. Wolfender,[a] Milena Botelho Perreira Soares,[cd] Pierre-Alain Carrupt[a] and Alessandra Nurisso*[a]

Received 7th May 2013,
Accepted 29th May 2013

DOI: 10.1039/c3mb70180h

www.rsc.org/molecularbiosystems

Trypanosoma cruzi and *Leishmania* spp. are protozoan pathogens responsible for Chagas disease and leishmaniasis, respectively. Current therapies rely only on a very small number of drugs, most of them are inadequate because of their severe host toxicity or drug-resistance phenomena. In order to find therapeutic alternatives, the identification of new biotargets is highly desired. In this study, homology modelling, docking and molecular dynamics simulations have been used to generate robust 3D models of NAD^+-dependent deacetylases from *Trypanosoma* and *Leishmania* spp., known as SIR2rp3, whose structures have never been described before. Molecular docking of known inhibitors revealed strong analogies with the mitochondrial human SIRT5 in terms of binding mode and interaction strength. On the other hand, by extending the analysis to the channel rims, regions of difference between host and parasitic targets, useful for future selective drug design projects, were pointed out.

Introduction

Chagas disease and leishmaniasis are caused by *Trypanosoma cruzi* and *Leishmania* spp. parasites, respectively, both belonging to the Trypanosomatidae family. In 2008, Chagas disease affected approximately 8–9 million individuals, causing around 14 000 deaths.[1] On the other hand, there are approximately 2 million new cases reported annually for leishmaniasis, with 350 million people considered at risk.[2] Visceral leishmaniasis can lead to death if not treated, whereas Chagas disease may evolve to chronic symptomatic forms with severe clinical manifestations, being a major cause of death by heart failure in Latin American countries.[3] To date, there have been no available human vaccines against such pathologies. The current treatments for Chagas disease (nifurtimox and benznidazol)[4,5] and for leishmaniasis (miltefosine, pentavalent antimony, and paronomycin) have many limitations including low efficacy, high toxicity, high cost and increasing resistance mechanisms. To date, only liposomal amphotericin B exhibits a good pharmacological profile, but the drug has other limitations including high toxicity and cost.[4,6–8] Therefore, there is an urgent need to develop new and safe therapies.

Sirtuin proteins, one of the most promising targets widely studied in the past decade, have been classified into five different classes (I, II, III, IV and U), depending on the presence of specific conserved motifs in their core domain.[9] Whereas genes from human genome encode for seven sirtuin proteins distributed in all classes with the exception of class U,[9] parasites from *Trypanosoma* and *Leishmania* both having three sirtuin genes, SIR2rp1, SIR2rp2 and SIR2rp3, the first one encoding for a class I sirtuin and the other two for class III sirtuins.[10]

Parasitic class I sirtuins, characterized by the GAGXSXXX-GIP**DF**RS, P**S**/TXXH, TQN**I**D, HG motifs,[9] have been extensively and successfully explored as antiparasitic targets.[10] It was demonstrated that such proteins play a key role in parasite survival by catalyzing the reaction of deacetylation of acetylated lysine residues belonging to parasite natural substrates such

[a] *Pharmacochemistry and Phytochemistry & Bioactive Natural Products, School of Pharmaceutical Sciences, University of Geneva, University of Lausanne, Quai Ernest-Ansermet 30, CH-1211 Geneva 4, Switzerland. E-mail: alessandra.nurisso@unige.ch*
[b] *Laboratory of Molecular Parasitology, Microbiology Dept, Hellenic Pasteur Institute, 127 Vasilissis Sofias avenue, 11521 Athens, Greece*
[c] *Centro de Pesquisas Gonçalo Moniz, Fundacão Oswaldo Cruz, Rua Waldemar Falcão, 121, Candeal 40296710, Salvador, BA, Brazil*
[d] *Hospital São Rafael, Av. São Rafael, 2152, São Marcos 41253190, Salvador, BA, Brazil*

† Electronic supplementary information (ESI) available: Procheck graphs; overall 3D structures; cavity depth and electropotential surfaces; molecular dynamics plots; homology modeling, docking and molecular dynamics details summarized in tables. Homology models are deposited in the Protein Model Database PMDB:[54] PM0078446 (*Tc*SIR2rp3), PM0078448 (*Lb*SIR2rp3). SIR2rp3 from *L. infantum* (*Li*SIR2rp3) was also built by following the same strategy. The model is accessible in the PMDB (code PM0078447). See DOI: 10.1039/c3mb70180h

as nuclear histones and other substrates, with NAD^+ as a cofactor.[11,12] Moreover, by interacting with parasite microtubules located in the cytoplasm, they participate in the remodelling of parasite morphology and in the interactions with host cells.[13] Nicotinamide and sirtinol have been demonstrated to be potent sirtuin inhibitors, unfortunately with no selectivity towards parasites.[14,15] Differences between human and parasitic sirtuins have been highlighted using molecular modeling[16–18] but an experimental support is still missing.[19]

Class III sirtuins are characterized by the GAGISAESGXPTFRG, PNXXH, TQNVD, HG motif.[9] The prototype mammalian member of this class is the human SIRT5, a mitochondrial enzyme having unique and potent demalonylase and desuccinylase activities.[20,21] Malonyl-lysine and succinyl-lysine occur in a wide range of eukaryota, from yeast to human.[21] Malonylation and succinylation have been detected in metabolic enzymes, including isocitrate dehydrogenase 2, serine hydroxylmethyltransferase, glyceraldehyde 3-phosphate dehydrogenase and others.[22] Mice lacking SIRT5 showed global protein hypermalonylation and hypersuccinylation, suggesting its fundamental role in such activities.[21] Thus, these post-translational modifications are expected to have a fundamental role in metabolism regulation. SIRT5 also regulates the carbamoyl phosphate synthetase 1 CPS1 function, an enzyme taking part in the urea cycle, through its deacetylase activity and desuccinylation.[23–25] Whereas nicotinamide was shown to inhibit desuccinylase activity in human SIRT5, the same compound surprisingly exhibited no effects on the deacetylase function. This phenomenon has been associated with the presence of a conserved Arg pointing toward the active site pocket and probably interfering with the nicotinamide binding orientation during the inhibition mechanism.[26]

Phylogenetic analysis indicated that trypanosomatid SIR2rp2 and SIR2rp3 proteins are related to the human mitochondrial protein SIRT5.[27,28] Interestingly, the NAD^+-dependent deacetylase encoded by the gene Tc00.1047053447255.20 isolated from *T. cruzi* (*Tc*SIR2rp3) has recently been considered as a challenging biotarget for the development of new anti-*T. cruzi* compounds.[29] However, no structural information could be found in the literature.

In this study, homology modelling, molecular docking and Molecular Dynamics (MD) simulation approaches will be used for building a high-quality three-dimensional 3D model of this enzyme. By following the same strategy, the protein encoded by the syntenic gene LbrM_20_1640 from *Leishmania* spp. (*Lb*SIR2rp3), will also be modelled.

Molecular docking of pan-sirtuin inhibitors (nicotinamide and sirtinol) and specific class III sirtuin inhibitors (thiobarbiturate derivatives) will be performed, interactions and energies compared. Finally, structural differences between mitochondrial human and parasitic proteins will be highlighted to finally provide robust structural information useful for the design of new antiparasitic and selective compounds.

Materials and method

Homology modelling: target and template retrieval

The primary sequences of NAD^+-dependent deacetylases from *T. cruzi* (*Tc*SIRrp3, Q4CNV0) and *L. braziliensis* (*Lb*SIRrp3, A4HAS6) were retrieved from the Universal Protein Resource (http://www.uniprot.org/) and used as targets for homology modelling. In order to find an appropriate template structure, each sequence was subjected to a PSI-BLASTp search (http://blast.ncbi.nlm.nih.gov/) against the Protein Data Bank PDB (http://www.rcsb.org/) by using the Blossum 62 matrix with an *E*-value cutoff of 10. Template search highlighted similarity with the *E. coli* CobB protein (PDB code 1S5P, 1.9 Å resolution), sharing ~60% sequence identity with the targets. However, due to the lack of resolution of the conserved GXPTFR motif in the template structure, the crystal structure of a sirtuin from *Archaeoglobus fulgidus* (PDB code 1ICI, 2.1 Å resolution) co-crystallyzed with NAD^+ was used as a template for modelling this loop (Fig. 1). A multi-template homology modelling approach was chosen and conducted in the MOE environment version 2011.10 (Chemical Computing Group CCG, Canada).

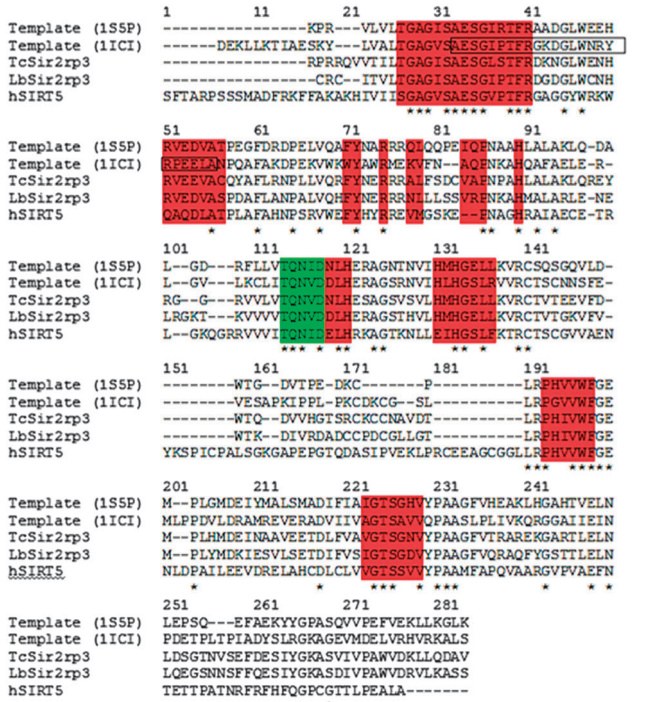

Fig. 1 Multiple sequence alignment between *Tc*SIR2rp3, *Lb*SIR2rp3, sirtuin from *E. coli* (PDB code 1S5P), sirtuin from *Archaeoglobus fulgidus* (PDB code 1ICI) and hSIRT5 (PDB code 3RIY). Amino acids in a 10 Å radius sphere around the ligand are shaded in red whereas the nicotinamide recognition sequence is shaded in green. Identity between amino acids is marked with an asterisk. Amino acids in the rectangular box were those used to model the loop in place of the ones from the *E. coli* sirtuin.

Homology modelling: construction and validation

Target-template alignments were performed by using the modified Needleman and Wunsch alignment methodology[30] implemented in the MOE-Align panel. The Blossum62 matrix was used for the alignment with a gap penalty of 5/10 for sequence/structural alignment options and a gap extend of 1 for both alignment options. Sequence alignments were finally fine-tuned manually. The MOE homology modelling module was then employed to build thirty intermediate models and one average model, all optimized using an Amber 99 force field[31] with a Reaction Field treatment

of solvation electrostatics. All thirty one models were checked by using the Procheck module[32] available on line at website http://nihserver.mbi.ucla.edu/. The ones with best structural features and geometry were selected and further refined through staged-energy minimizations conducted by using the Tripos force field[33] and Gasteiger–Huckel charges in SYBYLx 1.3 (Tripos Inc., St Louis, MO). PROCHECK was used again to assess the quality of the final models.

Molecular docking

The crystal structure of the bacterial sirtuin from *T. maritima* co-crystallized with nicotinamide[34] (PDB code 1YC5) was taken into account as reference, also for validating the docking methodology. This structure was prepared for docking in SYBYLx 1.3 by removing the crystallized water molecules, by adding the missing hydrogen atoms and by extracting the ligand. Ligand atom types were assigned according to the Tripos force-field.[33] The binding site was defined by a 10 Å radius sphere around the center of the pocket. Re-docking was then conducted by generating 100 docking solutions each one retrieved from 100 000 GOLD Genetic Algorithm iterations (preset option). Docking poses were evaluated and ranked according to the GoldScore. Root-mean-square-deviation (RMSD) values between the docking solutions and the crystallized ligand of reference were also calculated. By using the same docking protocol, nicotinamide, sirtinol[35] and two thiobarbiturate derivatives[36] were built in SYBYLx 1.3 and then docked into the human and modelled NAD^+-dependent deacetylases. Arg60 (*Tc*SIR2rp3), Arg59 (*Lb*SIR2rp3) and Arg105 (hSIRT5), key residues for the desuccinylase/deacetylase activities in the presence of nicotinamide,[37] were allowed to be flexible according to the GOLD library rotamers.

Molecular dynamics simulations

Selected docking poses were used as starting points for explicit-water MD simulations. Complexes were prepared using the tLeap module of Amber11.[38] Parameters for protein and nicotinamide were taken from Amberff99SB[39] and Gaff force fields,[40] respectively. Charges for inhibitors, compatible with Gaff, were calculated with the AM1-BCC method by using the Antechamber module.[41] Each complex was then embedded in an octahedral box of TIP3P water molecules (10 Å around the solute),[42] neutralized with Na^+/Cl^- ions and minimized using the *pmemd* module of Amber12.[38] The solvated complex was then free to relax along further 1500 steps of conjugate gradient and 1000 steps of steepest descent energy minimization. Systems were then equilibrated through 100 ps of slow heating at constant volume (from 10 K to 300 K) with weak restraints on the solute (10.0 kcal mol^{-1} $Å^{-1}$), followed by 50 ps MD under constant pressure conditions (1 atm). 700 ps without restraints allows us to reach the equilibrium of all systems, monitoring, with the *ptraj* module of Amber12, energies, pressure, density and RMSD values.[38] Trajectories were then collected each 2 ps along 4 ns of the MD production phase. All MD calculations were performed by applying boundaries conditions. The Particle-Mesh-Ewald algorithm (PME) with a cut-off of 8 Å was used for treating the long range electrostatic effects.[43] A SHAKE algorithm was also employed to constrain the bonds connecting hydrogen atoms.[44]

Analysis of molecular dynamics trajectories

MD trajectories were analyzed using the *ptraj* module of Amber12.[38] Fluctuations of ligand-bound complexes were monitored through the calculation of *b*-factor and RMSD values, by considering, as reference, the initial equilibrate structure extracted from each MD production phase.

The binding free energies (ΔG) between a ligand and a receptor to form a complex are calculated by using a MM-GBSA[45] and a normal mode[46] single trajectory approach at 300 K. Such methods require multiple snapshots from MD trajectories, from which water molecules are removed. For each single snapshot, the contribution of the solute internal energy is estimated through the molecular mechanics force field whereas the electrostatic and the non-polar solvation energy terms are calculated by applying the Generalized Born model[47] and by a solvent accessible surface area-based approach,[38] respectively. In this study, 1000 snapshots, taken every 2 ps, were extracted along 4 ns of the production phase. Due to the high computational demand, the entropic term was evaluated for 10 snapshots by performing a normal mode analysis using the *nmode* module of Amber12.[38] Binding free energy averages over the extracted snapshots were then considered to be final ΔG results.

Solvent accessible surface analyses

The homology models were then superimposed on the human sirtuin SIRT5[20] (hSIRT5, PDB code 3RIY) by using the nicotinamide recognition sequence (TQNXD motif) as reference for superimposition. Connolly surfaces were then generated for each protein by using the MOLCAD program[48] implemented in SYBYLx 1.3. Lipophilic and electrostatic potentials together with cavity depth properties were calculated on the surfaces and compared.[49]

Results and discussion

Construction and description of SIR2rp3 proteins from *T. cruzi* and *L. braziliensis*

In order to retrieve 3D information on *Tc*SIR2rp3 and *Lb*SIR2rp3 using homology modelling, a template search was carried out. The X-ray structure of the sirtuin from *E. coli* CobB (PDB code 1S5P) revealed to be the best choice for the modelling because of its percentage of identity with the targets and its belonging to the sirtuin class III. The identity between each target and the template was 56.8% and 53.9% for *Tc*SIR2rp3 and *Lb*SIR2rp3, respectively. The sequence alignment showed that the most conserved regions were mainly located at the NAD^+ recognition site (Fig. 1). Two homology models were successively built and refined. 100% of residues belonging to *Tc*SIR2rp3 and *Lb*SIR2rp3 occupied the allowed regions of the Ramachandran plot (Fig. S1, ESI†).

The typical folding characterizing proteins from the sirtuin family was retrieved in the three homology models: a large domain, a small domain and two long flexible loops, able to connect and to preserve the position of the two domains.[50] This loop also enclosed the catalytic site formed by three conserved pockets named A, B and C. Pocket A is known to interact with the adenosine–ribose motif of NAD^+. Pocket B interacts with

the nicotinamide–ribose motif and pocket C is responsible for the specific recognition of nicotinamide, containing the characteristic TQNXD motif (Fig. S2, ESI†).[50]

Molecular docking validates SIR2rp3 pockets and reveals analogies with the mitochondrial sirtuin hSIRT5

Molecular docking validation. In order to further validate the binding pockets of the modeled proteins, a molecular docking study was carried out by taking into account the pan-sirtuin inhibitor nicotinamide.[51] The docking methodology was first validated by re-docking nicotinamide into the *T. maritima* structure (PDB code 1YC5). All docking solutions were able to reproduce the crystallographic data. A RMSD value of 0.5 Å between the best ranked and the crystallographic nicotinamide pose was retrieved (Fig. S3, ESI†). Four hydrogen bonds characterized the interactions between the ligand and the protein:[34] two between the aromatic nitrogen of nicotinamide and the backbone of Phe33 and Pro31, respectively; one between the carboxyl group of nicotinamide and the backbone of Ile100 and one between the amide nitrogen of nicotinamide and the side chain of Asp101 from the TQNXD recognition sequence. Moreover, van der Waals interactions were observed between nicotinamide and side chains of Ile100, Phe33, Ile30 and Ala24 residues.

Docking of known inhibitors into the SIR2rp3 catalytic pockets. To validate the active site conformation of the modelled trypanosomatidae proteins, four known inhibitors were chosen for docking. Nicotinamide and sirtinol, two non-specific sirtuin inhibitors,[35,36] together with two thiobarbiturate derivatives, named 2 and 6, targeting the class III sirtuins.[36] Docking studies were conducted on both human and protozoan proteins in order to highlight analogies or differences in binding modes and interaction strength.

Among all the nicotinamide poses generated by using the GOLD genetic algorithm, the ones with the best overlap with the structural information coming from the *T. maritima* co-crystal were selected for further investigations (Table 1). The position of nicotinamide in the pockets showed conserved key interactions (Fig. 2A). Indeed, slight differences were observed: the backbone N atom of Val residues, replacing the human Ile169 residue, formed a hydrogen bond with the carboxyl group of the ligand in all parasitic proteins. Analogously, the Asp residue of the nicotinamide recognition sequence made polar contacts with the amide nitrogen atom of nicotinamide. Moreover, a π-stacking interaction with a conserved Phe residue, known to be essential for assuming an enzymatic productive state,[52] was retrieved in all parasitic docking poses. Further van der Waals contacts between Val and Ala residues forming the C-pocket and the nicotinamide ring were finally observed (Table S1, ESI†).

Docking calculations were also conducted on hSIRT5: nicotinamide interacted with the protein through two hydrogen bonds, a π-stacking and van der Waals contacts (Fig. 2A and Table S1, ESI†). The rigidity of the conserved Arg residue in the modelled C-pockets prevented the recovery of meaningful nicotinamide poses by docking (data not shown). In contrast, docking runs conducted with free Arg side chains allowed the collection of docking solutions comparable to structural data coming from the literature.[34,52] Interestingly, Arg side chains adopted the same conformation in all proteins (κ_1: −67°, κ_2: 180°, κ_3: 65° and κ_4: −175°). Rotili *et al.* described the orientation of sirtinol in the sirtuin catalytic pocket, reminding the orientation of the cofactor NAD^+.[53] The hydroxynaphthalene ring of sirtinol seems to occupy the site A of the pocket while the central benzene interacts with the site B and the terminal benzene cycle with the site C, assuming a conformation similar to the pyridine ring of NAD^+.

Docking pose analysis revealed that such orientation is well conserved in both human and parasitic proteins (Fig. 2B). Interactions with key amino acid already described in the literature[52] were retrieved, in particular regarding the C site where Ile142, Ala59 and Phe70 (hSIRT5), Val97, Ala14 and Phe25 (*Tc*SIR2rp3), Val97, Ala13 and Phe24 (*Lb*SIR2rp3) make hydrophobic contacts with the terminal benzene ring of sirtinol. Hydrophobic interactions between two conserved Gly residues of the site A and the naphthalene ring of the sirtinol should also be mentioned (Table S1, ESI†). Interestingly, GoldScore for the sirtinol poses was close to the ones obtained for nicotinamide (Table 1). These results seem to be in accordance with IC_{50} obtained in hSIRT5 for nicotinamide and sirtinol which indicate similar affinities of the two ligands for hSIRT5.[36]

The orientation of the thiobarbiturate compound 2 in both parasitic and human sirtuins is well reproduced if compared to the one described by Maurer *et al.*[36] Key hydrogen bonds with Arg105 and Tyr102 (hSIRT5), Arg60 and Tyr57 (*Tc*SIR2rp3) and

Table 1 IC_{50} from the literature,[36] GoldScore values obtained by docking and binding free energies ΔG_{bind} (kcal mol^{-1}) obtained using the MM-GBSA coupled nmode approach for nicotinamide, sirtinol, thiobarbiturate 2 and 6 in complex with hSIRT5, *Tc*SIR2rp3 and *Lb*SIR2rp3. Standard deviations are reported in brackets

Nicotinamide	hSIRT5	*Tc*SIR2rp3	*Lb*SIR2rp3	Sirtinol	hSIRT5	*Tc*SIR2r3	*Lb*SIR2r3
IC_{50}	46.6 (3.0)	—	—	IC_{50}	48.9 (6.3)	—	—
GoldScore	34.2	—	—	GoldScore	32.4	—	—
ΔG_{MMGBSA}	−14.3 (1.3)	−19.0 (1.8)	−11.6 (3.0)	ΔG_{MMGBSA}	−25.1 (5.2)	−25.0 (2.2)	−23.2 (8.2)
$-T\Delta S_{NMODE}$	13.9 (3.4)	15.9 (0.5)	10.0 (3.0)	$-T\Delta S_{NMODE}$	23.9 (3.0)	22.1 (2.8)	21.6 (5.2)
ΔG_{bind}	−0.4	−3.2	−1.6	ΔG_{bind}	−1.2	−2.9	−1.6
Thiobarbiturate compound 2	hSIRT5	*Tc*SIR2rp3	*Lb*SIR2rp3	Thiobarbiturate compound 6	hSIRT5	*Tc*SIR2r3	*Lb*SIR2r3
IC_{50}	2.3 (0.2)			IC_{50}	16.6 (0.4)	—	—
GoldScore	62.3			GoldScore	58.8	—	—
ΔG_{MMGBSA}	−27.6 (3.5)	−30.0 (2.0)	−33.3 (2.8)	ΔG_{MMGBSA}	−32.6 (5.0)	−27.1 (2.4)	−37.0 (1.0)
$-T\Delta S_{NMODE}$	20.1 (0.8)	20.3 (1.6)	23.0 (1.8)	$-T\Delta S_{NMODE}$	26.5 (0.1)	22.7 (0.6)	19.7 (6.0)
ΔG_{bind}	−7.5	−9.7	−10.4	ΔG_{bind}	−6.1	−4.5	−17.3

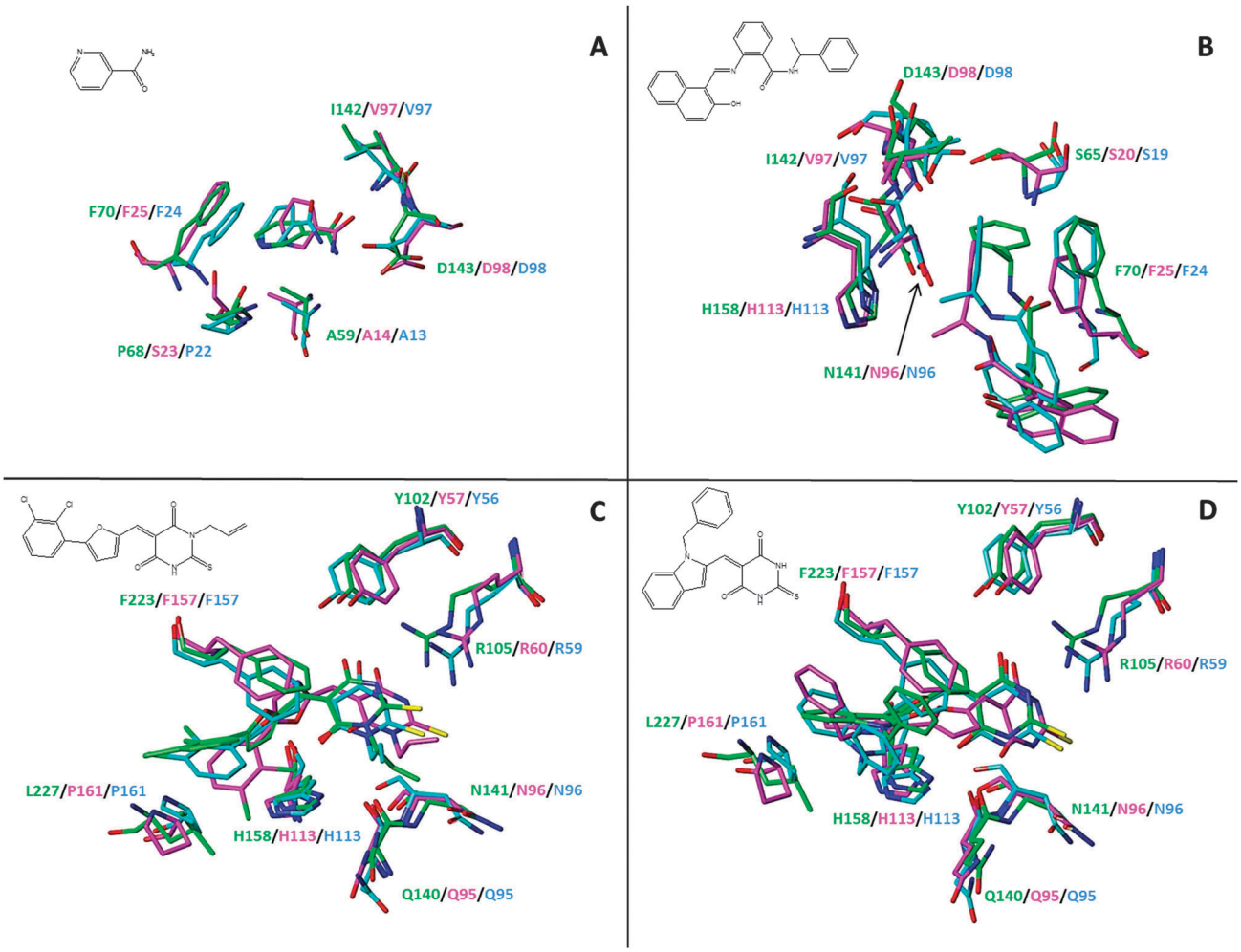

Fig. 2 Superimposition of nicotinamide (A), sirtinol (B), thiobarbiturate compound 2 (C) and thiobarbiturate compound 6 (D) docking poses in hSIRT5 (green carbon atoms), *Tc*SIR2rp3 (magenta carbon atoms) and *Lb*SIR2rp3 (cyan carbon atoms) proteins. Residues making contacts with the inhibitors are represented in capped sticks. 2D representation of each docked ligand is also reported.

Arg59 and Tyr56 (*Lb*SIR2rp3) can be observed (Fig. 2C). Moreover, hydrophobic interactions between the aromatic ring of the compound and Phe223 and His158 residues belonging to the lysine substrate channel of hSIRT5 can also be observed. Such interactions are retrieved in the protozoan proteins: Phe157 and His113 (*Tc*SIR2rp3 and *Lb*SIR2rp3). Docking score analysis revealed that this ligand seems to have more affinity towards the proteins than nicotinamide and sirtinol (Table 1). This observation is in line with the lower IC_{50} obtained for this ligand in hSIRT5.[36]

Thiobarbiturate compound 6 was finally docked into the three structures (Fig. 2D). As for thiobarbiturate 2, docking scores revealed a better affinity of this ligand for the proteins than nicotinamide. The overall orientation of this ligand together with the contacts observed for compound 2 was herein conserved. Therefore, slight differences in IC_{50} values between compound 2 and 6 in hSIRT5, also in line with the obtained GoldScore values, were observed.[36] This behaviour may be due to a better accommodation of the hydrophobic moiety characterized by chlorine substituents of compound 2 in the pocket and to the fact that the terminal aromatic ring of compound 6 points toward the solvent, destabilizing, with its flexibility, the interaction with the protein.

Sirtuin–inhibitor complexes: stability and energies from molecular dynamics MD simulations

Complexes obtained using docking calculations were then studied using MD simulations in order to check their stability over time in a hydrated environment. The systems were embedded in explicit water molecules, neutralized and extensively minimized, reaching an equilibrium state after 850 ps of MD (Fig. S4 and Table S2, ESI†). 4 ns trajectories in which the systems were free to move were then collected and protein motions evaluated. Atoms belonging to inhibitors and backbone atoms remained relatively stable along all the production phases, with RMSD values lower than 2 Å (Fig. 3, Fig. S6 and Table S3, ESI†). Moreover, low *b*-factor values were obtained for those aminoacid residues directly involved in the binding (Fig. S5, ESI†). The small fluctuations during the simulations indicate the stability of the modelled complexes over the entire

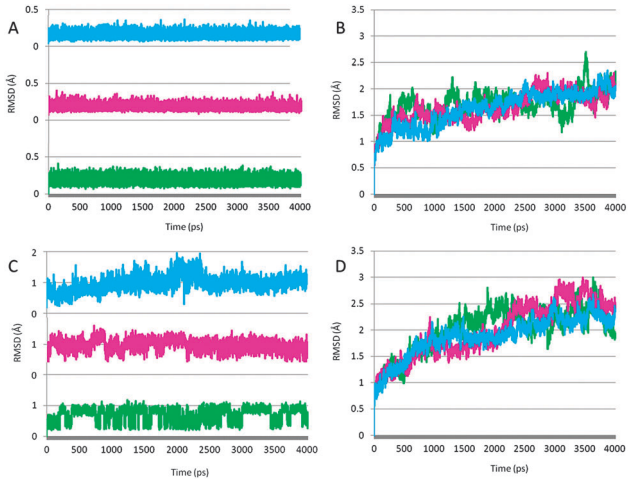

Fig. 3 RMSD plots against time calculated for the atoms belonging to: nicotinamide (A); thiobarbiturate compound 2 (B); backbone atoms of the proteins in complex with nicotinamide (C) and with thiobarbiturate compound 2 (D). hSIRT5, *Tc*SIR2rp3 and *Lb*SIR2rp3 are colored in green, magenta and cyan, respectively.

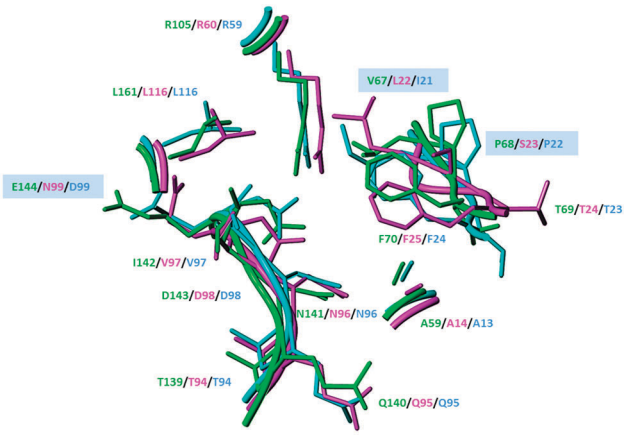

Fig. 4 Superimposition of the active sites of human and parasitic NAD^+-dependent deacetylases. Atoms are represented in capped sticks and colored in green (hSIRT5, PDB code 3RIY), magenta (*Tc*SIR2rp3) and cyan (*Lb*SIR2rp3). Punctual differences are shaded in light blue.

trajectories, able to guarantee a reliable basis for further thermal investigations.

Binding free energies (ΔG_{bind}) were then calculated for 2000 snapshots extracted from MD production phases of each simulation with a MM-GBSA coupled normal mode approach. The final energies, summarized in Table 1, revealed favourable bound states between inhibitors and modelled proteins, with negative values (kcal mol^{-1}) comparable to the ones obtained for the modelling-based inhibitor–hSIRT5 complexes. Moreover, the calculated energetic values respect the tendencies of specificity towards the class III sirtuin (increasing affinity of thiobarbiturate derivatives in SIR2rp3 pockets) and also the IC_{50} trend estimated for hSIRT5.[36]

Taken together, molecular docking and MD results provide evidence on the robustness of the three homology models. Moreover, they highlight strong analogies between Sir2rp3 proteins and human SIRT5, suggesting and reinforcing the idea of a mitochondrial function and localization of such parasitic proteins.[19] Experimental evidence about SIR2rp3 localization has been reported in the past only for *T. brucei*.[28] The high percentage of sequence identity between *Tb*SIR2rp3, *Tc*SIR2rp3, *Li*SIR2rp3 and *Lb*SIR2rp3 (Table S4, ESI†), especially at the pocket level (~60% Fig. S7 and Table S5, ESI†), seems to confirm the hypothesis.

Selectivity towards parasites: observation from structural and solvent accessible surface analyses

To reduce adverse effects on patients, a selective activity of candidate drugs towards parasitic enzymes may be desired. Among the human enzymes, the mitochondrial class III sirtuin hSIRT5 has been shown to be the closest one to the modelled proteins (Table S4, ESI†) as also highlighted through molecular docking and MD calculations.[19] As shown in Fig. 4 and Table S5 (ESI†), C pocket residues are highly conserved among the species, especially the TQNXD nicotinamide recognition sequence and the Arg residue, known for being responsible for nicotinamide inhibition resistance phenomena.[19,22]

In order to better visualize the C site, being the main interaction area with known inhibitors,[29,52] each homology model as well as hSIRT5 were superimposed to the sirtuin form *T. maritima* co-crystallized with nicotinamide[34] (PDB code 1YC5). By considering an area of 6 Å around the ligand, only Glu144 of hSIRT5 was found to be mutated in Asp and Asn residues in the parasitic enzymes. Pro68 from hSIRT5 was conserved in *Lb*SIR2rp3 but not in *Tc*SIR2rp3 in which a polar Ser23 residue can be found. Ile142 from hSIRT5 was replaced by Val residues in the parasites, conserving the punctual apolar features. Solvent accessible surfaces were then created for each protein and cavity depth, lipophilic and electrostatic properties calculated in order to compare and analyse the properties of the whole catalytic channels. A similar strategy was adopted in the past for highlighting differences between human and parasitic SIR2rp1 proteins.[16,17]

The cavity depth analysis provided comparable depth values (~11 Å) among proteins. Moreover, dimensions and shapes of both human and parasitic catalytic channels presented great similarity (Fig. S8, ESI†). In order to quantify this observation, four regions, A–D, representing the boundaries of the catalytic rim of each enzyme, were defined and distances between them measured (Table S6, ESI†). Such similarities can be explained by the relatively good percentage of identity between hSIRT5 and parasitic SIR2rp3 (~35%, Table S4, ESI†) mainly localized in this specific area (Table S4, ESI†). It should be mentioned that the homology models were built by using the sirtuin from *E. coli* CobB (PDB code 1S5P) as a main template: this protein is a class III sirtuin, as both human and parasitic proteins taken into account in this study (Table S4, ESI†). Moreover, the modelling of the loop enclosing the conserved GIXTFR motif was based on the structure from *Archaeoglobus fulgidus* (PDB code 1ICI), crystallized, as hSIRT5, in a relatively productive conformation state. Productive conformation was recently described by Sakkiah *et al.* illustrating the essential

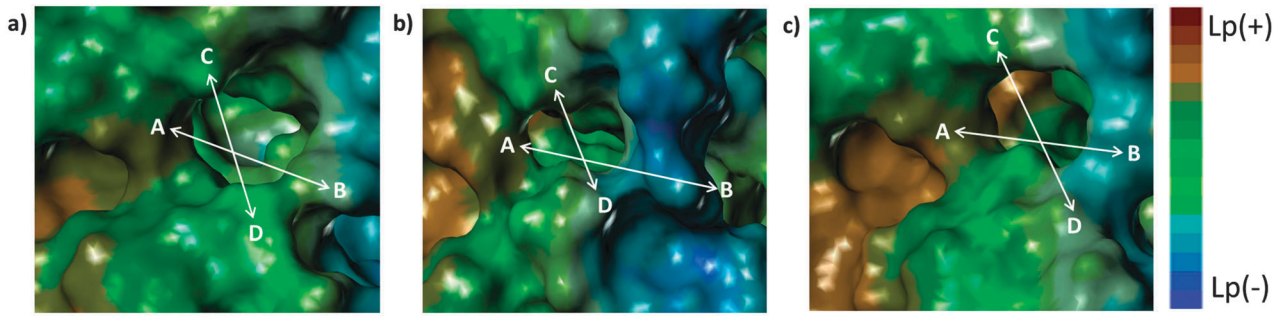

Fig. 5 Lipophilic properties calculated on the solvent accessible surface of hSIRT5 (a), *Tc*SIR2rp3 (b) and *Lb*SIR2rp3 (c). Surfaces are color-coded according to the lipophilic potential Lp from brown (highest hydrophobic area) to blue (highest hydrophilic area). The rim channels are characterized by four regions named A, B, C and D.

conformational changes that sirtuin proteins undergo when in complex with ligands.[52]

The lipophilic properties of the sirtuin channel rims are shown in Fig. 5. By visual inspection, it is easy to notice common lipophilic features with few exceptions. The zone enclosed between B and D areas, including the conserved Arg residue,[9,52] is characterized by the hydrophobic Val253 residue in hSIRT5 that is replaced by Asp185 in *Lb*SIR2rp3 and by an Asn residue (Asn185) in *Tc*SIR2rp3 proteins. Whereas acid residues are conserved in the C sirtuin regions (Glu38 in *Tc*SIR2rp3, Asp38 in Leishmania proteins, and Asp84 in hSIRT5), polar Lys28 and Ser27 residues in *Tc*SIR2rp3 are mutated in Gly27 and Ala73 in *Lb*SIR2rp3 and hSIRT5 respectively. In addition, a Glu residue found in all parasitic protein is replaced by Gln83 in hSIRT5. This specific region of diversity can also be observed when the electrostatic potential is calculated and visualized on the surfaces. In effect, the C region of hSIRT5 assumes relatively neutral properties in this specific area, in contrast to the corresponding electronegative blue ones of the parasitic proteins (Fig. S9, ESI†). Table S7 (ESI†) summarizes the amino acids characterizing such regions of diversity.

Conclusion

Meaningful 3D models of parasitic SIR2rp3 proteins, new targets for the development of candidate drugs against Chagas disease and leishmaniasis, were generated. These structures, refined and validated by means of complementary molecular modelling techniques, were described here in detail for the first time.

Through molecular docking and molecular dynamics simulations, similar binding modes of two pan-sirtuin inhibitors, nicotinamide and sirtinol, and two thiobarbiturate compounds, targeting the class III sirtuin family, were obtained. Such results indicated a certain degree of analogy between proteins that further support the hypothesis on localization and a role of the three modelled protozoan proteins.

Since the design of new inhibitors specifically targeting the parasites is desired, a structural and a physicochemical property-based comparison of catalytic pockets with the homologous human protein hSIRT5 from mitochondria allowed the identification of minor but significant differences. Thanks to the information retrieved from this study, the search for compounds with inhibitory and species-specific properties could be potentially directed towards relatively hydrophobic scaffolds with electron-rich or electropositive moieties matching the B–D areas of diversity of *Tc*SIR2rp3 and *Lb*SIR2rp3 catalytic rims, respectively. Polar groups could also be added to the main scaffold for matching the hydrophilic C region of parasitic targets. A graphical schema summarizing these observations is reported in Fig. S10 (ESI†). Taken together, these results provide strong basis for directing future structural-based drug design projects concerning SIR2rp3 that, together with the information already known about parasitic SIR2rp1, can be useful in the discovery of new selective compounds active against trypanosomiasis and leishmaniasis.

Acknowledgements

The authors thank researchers from the CHEMBIOFIGHT project (EC/FP7/269301) for valuable scientific discussions. The authors are grateful to the Swiss National Science Foundation for financial support.

Notes and References

1 P. J. Hotez, M. E. Bottazzi, C. Franco-Paredes, S. K. Ault and M. R. Periago, *PLoS Neglected Trop. Dis.*, 2008, **2**, e300.
2 World Health Organization Report, 2000, 1–109.
3 World Health Organization Report, 2010, 1–186.
4 S. Kappagoda, U. Singh and B. G. Blackburn, *Mayo Clin. Proc.*, 2011, **86**, 561–583.
5 W. Apt, *Drug Des., Dev. Ther.*, 2010, **4**, 243–253.
6 K. Seifert, *Open Med. Chem. J.*, 2011, **5**, 31–39.
7 S. R. Wilkinson, M. C. Taylor, D. Horn, J. M. Kelly and I. Cheeseman, *Proc. Natl. Acad. Sci. U. S. A.*, 2008, **105**, 5022–5027.
8 S. L. Croft, K. Seifert and V. Yardley, *Indian J. Med. Res.*, 2006, **123**, 399–410.
9 R. A. Frye, *Biochem. Biophys. Res. Commun.*, 2000, **273**, 793–798.
10 A. A. Religa and A. P. Waters, *Mol. Biochem. Parasitol.*, 2012, **185**, 71–88.
11 B. Vergnes, D. Sereno, N. Madjidian-Sereno, J. L. Lemesre and A. Ouaissi, *Gene*, 2002, **296**, 139–150.

12 X. Li and N. Kazgan, *Int. J. Biol. Sci.*, 2011, **7**, 575–587.
13 J. Tavares, A. Ouaissi, N. Santarem, D. Sereno, B. Vergnes, P. Sampaio and A. Cordeiro-Da-Silva, *Biochem. J.*, 2008, **415**, 377–386.
14 J. Tavares, A. Ouaissi, P. Kong Thoo Lin, I. Loureiro, S. Kaur, N. Roy and A. Cordeiro-Da-Silva, *ChemMedChem*, 2010, **5**, 140–147.
15 B. Vergnes, D. Sereno, J. Tavares, A. Cordeiro-Da-Silva, L. Vanhille, N. Madjidian-Sereno, D. Depoix, A. Monte-Alegre and A. Ouaissi, *Gene*, 2005, **363**, 85–96.
16 S. Kaur, A. Shivange and N. Roy, *Mol. Diversity*, 2010, **14**, 169–178.
17 R. U. Kadam, V. M. Kiran and N. Roy, *Bioorg. Med. Chem. Lett.*, 2006, **16**, 6013–6018.
18 R. U. Kadam, J. Tavares, V. Kiran, A. Cordeiro, A. Ouaissi and N. Roy, *Chem. Biol. Drug Des.*, 2008, **71**, 501–506.
19 W. Zheng, *Eur. J. Med. Chem.*, 2012, 132–140.
20 J. Du, Y. Zhou, X. Su, J. J. Yu, S. Khan, H. Jiang, J. Kim, J. Woo, J. H. Kim, B. H. Choi, B. He, W. Chen, S. Zhang, R. A. Cerione, J. Auwerx, Q. Hao and H. Lin, *Science*, 2011, **334**, 806–809.
21 C. Peng, Z. Lu, Z. Xie, Z. Cheng, Y. Chen, M. Tan, H. Luo, Y. Zhang, W. He, K. Yang, B. M. M. Zwaans, D. Tishkoff, L. Ho, D. Lombard, T. C. He, J. Dai, E. Verdin, Y. Ye and Y. Zhao, *Mol. Cell. Proteomics*, 2011, **10**, M111.012658.
22 J. C. Newman, W. He and E. Verdin, *J. Biol. Chem.*, 2012, **287**, 42436–42443.
23 T. Nakagawa, D. J. Lomb, M. C. Haigis and L. Guarente, *Cell*, 2009, **137**, 560–570.
24 T. Nakagawa and L. Guarente, *Aging*, 2009, **1**, 578–581.
25 W. He, J. C. Newman, M. Z. Wang, L. Ho and E. Verdin, *Trends Endocrinol. Metab.*, 2012, **23**, 467–476.
26 F. Fischer, M. Gertz, B. Suenkel, M. Lakshminarasimhan, M. Schutkowski and C. Steegborn, *PLoS One*, 2012, **7**, e45098.
27 J. A. Garcia-Salcedo, P. Gijon, D. P. Nolan, P. Tebabi and E. Pays, *EMBO J.*, 2003, **22**, 5851–5862.
28 S. Alsford, T. Kawahara, C. Isamah and D. Horn, *Mol. Microbiol.*, 2007, **63**, 724–736.
29 M. B. P. Soares, C. V. Silva, T. M. Bastos, E. T. Guimaraes, C. P. Figueira, D. Smirlis and W. F. Azevedo Jr, *Acta Trop.*, 2012, **122**, 224–229.
30 S. B. Needleman and C. D. Wunsch, *J. Mol. Biol.*, 1970, **48**, 443–453.
31 W. Junmei, P. Cieplak and P. Kollman, *J. Comput. Chem.*, 2000, **21**, 1049–1074.
32 R. A. Laskowski, M. W. MacArthur, D. S. Moss and J. M. Thornton, *J. Appl. Crystallogr.*, 1993, **26**, 283–291.
33 M. Clark, R. D. Cramer III and N. Van Opdenbosch, *J. Comput. Chem.*, 1989, **10**, 982–1012.
34 J. L. Avalos, K. M. Bever and C. Wolberger, *Mol. Cell*, 2005, **17**, 855–868.
35 M. Lawson, U. Uciechowska, J. Schemies, T. Rumpf, M. Jung and W. Sippl, *Biochim. Biophys. Acta*, 2010, **1799**, 726–739.
36 B. Maurer, T. Rumpf, M. Scharfe, D. A. Stolfa, M. L. Schmitt, W. He, E. Verdin, W. Sippl and M. Jung, *ACS Med. Chem. Lett.*, 2012, **3**, 1050–1053.
37 S. C. Lovell, J. M. Word, J. S. Richardson and D. C. Richardson, *Proteins: Struct., Funct., Genet.*, 2000, **40**, 389–408.
38 D. A. Case, T. E. Cheatham III, C. L. Simmerling, J. Wang, R. E. Duke, R. Luo, T. A. Darden, W. Zhang, K. M. Merz, B. Roberts, B. Wang, S. Hayik, R. C. Walker, G. Seabra, I. Kolossvary, K. F. Wong, F. Paesani, J. Vanicek, J. Liu, A. Roitberg, S. R. Brozell, T. Steinbrecher, H. Gohlke, Q. Cai, X. Ye, J. Wang, X. Wu, G. Cui, D. R. Roe, D. H. Mathews, M. G. Seetin, C. Sagui, V. Babin, J. J. Hsieh, S. Gusarov, A. Kovalenko, P. A. Kollman and T. Luchko, 2010.
39 V. Hornak, R. Abel, A. Okur, B. Strockbine, A. Roitberg and C. Simmerling, *Proteins: Struct., Funct., Bioinf.*, 2006, **65**, 712–725.
40 J. M. Wang, R. M. Wolf, J. W. Caldwell, P. A. Kollman and D. A. Case, *J. Comput. Chem.*, 2004, **25**, 1157–1174.
41 D. A. Case, T. E. Cheatham, T. Darden, H. Gohlke, R. Luo, K. M. Merz, A. Onufriev, C. Simmerling, B. Wang and R. J. Woods, *J. Comput. Chem.*, 2005, **26**, 1668–1688.
42 J. Aqvist, *J. Phys. Chem.*, 1990, **94**, 8021–8024.
43 T. Darden, D. York and L. Pedersen, *J. Chem. Phys.*, 1993, **98**, 10089–10092.
44 J. P. Ryckaert, G. Ciccotti and H. J. C. Berendsen, *J. Comp. Physiol.*, 1977, **23**, 327–341.
45 D. A. Case, T. A. Darden, T. E. Cheatham, C. L. Simmerling, J. Wang, R. E. Duke, R. Luo, R. C. Walker, W. Zhang, K. M. Merz, B. Roberts, S. Hayik, A. Roitberg, G. Seabra, J. Swails, A. W. Goetz, I. Kolossvai, K. F. Wong, F. Paesani, J. Vanicek, R. M. Wolf, J. Liu, X. Wu, S. R. Brozell, T. Steinbrecher, H. Gohlke, Q. Cai, X. Ye, J. Wang, M. J. Hsieh, G. Cui, D. R. Roe, D. H. Mathews, M. G. Seetin, R. Salomon-Ferrer, C. Sagui, V. Babin, T. Luchko, S. Gusarov, A. Kovalenko and P. A. Kollman, 2012.
46 B. Brooks and M. Karplus, *Proc. Natl. Acad. Sci. U. S. A.*, 1983, **80**, 6571–6575.
47 A. Onufriev, D. Bashford and D. A. Case, *Proteins: Struct., Funct., Bioinf.*, 2004, **55**, 383–394.
48 M. L. Connolly, *Science*, 1983, **221**, 709–713.
49 M. Keil, T. E. Exner and J. Brickmann, *J. Comput. Chem.*, 2004, **25**, 779–789.
50 M. S. Finnin, J. R. Donigian and N. P. Pavletich, *Nat. Struct. Biol.*, 2001, **8**, 621–625.
51 K. T. Andrews, A. Haque and M. K. Jones, *Immunol. Cell Biol.*, 2012, **90**, 66–77.
52 S. Sakkiah, M. Chandrasekaran, Y. Lee, S. Kim and K. W. Lee, *J. Biomol. Struct. Dyn.*, 2012, **30**, 235–254.
53 D. Rotili, D. Tarantino, A. Nebbioso, C. Paolini, C. Huidobro, E. Lara, P. Mellini, A. Lenoci, R. Pezzi, G. Botta, M. Lahtela-Kakkonen, A. Poso, C. Steinkühler, P. Gallinari, R. De Maria, M. Fraga, M. Esteller, L. Altucci and A. Mai, *J. Med. Chem.*, 2012, **55**, 10937–10947.
54 T. Castrignano, P. D'Onorio De Meo, D. Cozzetto, I. G. Talamo and A. Tramontano, *Nucleic Acids Res.*, 2006, **34**, D306–D309.

